



1 **SM2RAIN-CCI: A new global long-term rainfall data set derived**
2 **from ESA CCI soil moisture**

3 Luca Ciabatta^{1,4}, Christian Massari¹, Luca Brocca¹, Alexander Gruber², Christoph Reimer³,
4 Sebastian Hahn², Christoph Paulik², Wouter Dorigo², Richard Kidd³, Wolfgang Wagner²

5 ¹Research Institute for Geo-Hydrological Protection, National Research Council, Perugia, Italy

6 ²Department of Geodesy and Geoinformation, TU Wien, Vienna, Austria

7 ³Earth Observation Data Centre, Vienna, Austria

8 ⁴Department of Civil and Environmental Engineering, University of Perugia, Italy

9

10

11

12

13

14

15

16

17

18

19

20

21

22

23

24

25

26

27

28

29

30

31

32

33

34 *Correspondence to:* Luca Ciabatta (luca.ciabatta@irpi.cnr.it)



35 **ABSTRACT**

36 Accurate and long-term rainfall estimates are the main inputs for several applications, spanning from crop modeling to
37 climate analysis. In this study, we present a new rainfall data set (SM2RAIN-CCI) obtained from the inversion of the
38 satellite soil moisture (SM) observations derived from the ESA Climate Change Initiative (CCI) via SM2RAIN (Brocca
39 et al., 2014). Daily rainfall estimates are generated for an 18-year long period (1998-2015), with a spatial sampling of
40 0.25° on a global scale and are based on the integration of the ACTIVE and the PASSIVE ESA CCI SM data sets.

41 The quality of the SM2RAIN-CCI rainfall data set is evaluated by comparing it with two state-of-art rainfall satellite
42 products, i.e. the Tropical Measurement Mission Multi-satellite Precipitation Analysis 3B42 real-time product (TMPA
43 3B42RT) and the Climate Prediction Center Morphing Technique (CMORPH), and one modelled data set (ERA-
44 Interim). The assessment is carried out on a global scale at 1° of spatial sampling and 5-day of temporal sampling by
45 comparing these products with the gauge-based Global Precipitation Climatology Centre Full Data Daily (GPCC-FDD)
46 product. SM2RAIN-CCI shows relatively good results in terms of correlation coefficient (median value >0.56), Root
47 Mean Square Difference (RMSD, median value <10.34 mm) and BIAS (median value $<-14.44\%$) during the evaluation
48 period. The validation has been also carried out at original resolution (0.25°) over Europe, Australia and other 5 areas
49 worldwide to test the capabilities of the data set to correctly identify rainfall events under different climate and
50 precipitation regimes.

51 The CCI-SM derived rainfall data set is freely available at <http://www.esa-soilmoisture-cci.org> at
52 <https://doi.org/10.5281/zenodo.846259>.

53 **1 INTRODUCTION**

54 Accurate estimation of rainfall is of paramount importance for many applications, e.g. natural hazards risk assessment
55 and mitigation, famine and disease monitoring, water resources management, weather forecasting and climate
56 modelling (Dinku et al., 2007).

57 Ground stations provide very accurate local estimates of rainfall (Villarini et al., 2008) and are considered the most
58 accurate source of rainfall data for modelling and process monitoring. However, two main issues limit their usefulness.
59 Firstly, they are characterized by a non-homogenous coverage (Kidd et al., 2016) throughout the globe and, secondly,
60 they are only representative of a limited area around the gauge. These limitations impact the use of rain gauge data
61 mainly over large and remote areas. Another source of rainfall information are ground meteorological radars, which are
62 able to provide measurements that are more representative of the actual rainfall spatial variability. However, also
63 ground meteorological radars are affected by issues that reduce the quality of the rainfall estimates such as beam
64 blockage and frozen hydrometeors. In addition, ground-based observations are subjected to high costs of maintenance
65 related to setting up, calibration and fixing of raingauges and radars. These issues can limit the use of ground rainfall
66 estimates, especially in developing countries.

67 Satellite rainfall estimates can offer a valuable alternative to ground-based observations and today provide
68 measurements at an increased spatial and temporal resolution. For example, the recent NASA/JAXA joint Global
69 Precipitation Measurement (GPM, Hou et al., 2014) mission delivers rainfall products in near real-time with a spatial
70 sampling of 0.1° every 30 minutes, by using a constellation of satellite sensors. A large number of satellite rainfall
71 products have been developed in the past, e.g. the near-real-time Tropical Rainfall Measurement Mission Multi-satellite
72 Precipitation Analysis (TMPA 3B42RT, Huffman et al., 2007); the Precipitation Estimation from Remotely Sensed
73 Information using Artificial Neural Networks (PERSIANN, Hsu et al., 1997), the Climate Prediction Center



74 MORPHing technique, (CMORPH, Joyce et al., 2004), and the Climate Hazards Group InfraRed Precipitation with
75 Station, (CHIRPS, Funk et al., 2015) products. These products are being used worldwide for several applications, such
76 as drought and famine monitoring, weather forecasts and natural hazard risk mitigation. When providing a sufficiently
77 long observation period, they are also used for climatological applications like the PERSIANN-Climate Data Record
78 (Ashouri et al., 2015), which provides continuous rainfall estimates since 1983. Despite the relative advantages of
79 having an estimate of rainfall in every place of the earth, satellite rainfall estimates, like ground observations, are not
80 free of errors. In fact, the instantaneous satellite-based retrievals of precipitation, which is a process subject to high
81 spatial and temporal variability, makes the reconstruction of the accumulated rainfall at longer temporal scales (e.g.,
82 daily accumulated rainfall) challenging (Trenberth and Asram, 2014). Another issue is related to the estimation of light
83 rainfall, especially over land, which is impacted by the land surface emissivity (Kucera et al., 2013). These aspects
84 negatively affect the rainfall estimates at the measurement area limiting their use especially for operational purposes,
85 like natural hazards assessment. The use of a constellation of satellites, as adopted in the GPM mission, is able to
86 mitigate the issue of the accumulated rainfall estimation through more frequent satellite overpasses during a day, thus
87 reducing the errors associated with the retrievals (Panegrossi et al., 2016).

88 A way to improve the quality of satellite rainfall estimates has been explored recently by means of different approaches
89 and relies on the use of satellite surface soil moisture (SSM) data (Crow et al., 2009, 2011; Pellarin et al., 2013; Brocca
90 et al., 2013, 2014; Wanders et al., 2015; Zhan et al., 2015). These approaches exploit the strong relationship between
91 SSM and rainfall to correct and/or estimate rainfall by using satellite surface SM data. Among these methods,
92 SM2RAIN (Brocca et al., 2013) is the only technique that directly provides rainfall estimates from SSM observations
93 while the others are correction-based techniques. SM2RAIN has been used to estimate precipitation from various
94 single-sensor SSM products, e.g. from ASCAT, SMOS, etc... (Brocca et al., 2013, 2014, 2016; Ciabatta et al., 2015,
95 2017; Koster et al., 2016, Massari et al. 2017).

96 With the aim of facing and monitoring climate change, the European Space Agency (ESA) has established the so-called
97 Climate Change Initiative (CCI) project. The objective is to exploit Earth Observation data sets for providing useful
98 information to policy makers about several Essential Climate Variables (ECV). Within the CCI programme, three long-
99 term SM products (>37 years) have been developed by merging SSM retrievals from both active and passive microwave
100 instruments carried by various satellite platforms (Liu et al., 2011, Liu et al., 2012, Wagner et al., 2012). More
101 specifically, the CCI SM project provides three different products, namely Active (obtained by merging radar-estimated
102 SM), Passive (obtained by merging radiometer-estimated SM) and Combined (obtained by merging the Active and
103 Passive data sets). The availability of these SM data records opens up new opportunities for creating independent long-
104 term rainfall data sets based on SM2RAIN.

105 The objective of this study is to present and evaluate a quasi-global long-term SM2RAIN-CCI rainfall data set obtained
106 from the inversion of the ESA CCI SM via the SM2RAIN algorithm (Brocca et al., 2014). The SM2RAIN-CCI rainfall
107 data set is compared against several precipitation products, e.g. TMPA 3B42RT, CMORPH, ERA-Interim, the Global
108 Precipitation Climatology Centre Full Data Daily (GPCC-FDD) product (Schamm et al., 2015) and the recently
109 developed Multi-Source Weighted-Ensemble Precipitation (MSWEP, Beck et al., 2016). The analysis is performed on a
110 global scale at 1° spatial sampling, during the period 1998-2015. In addition, a regional scale analysis at 0.25° spacing
111 is performed by comparing SM2RAIN-CCI estimates against high quality ground-based observations over Europe,
112 India and Australia.



113 2 DATA AND METHODS

114 2.1 Data set generation

115 2.1.1 State-of-the-art rainfall data sets

116 In this study, five state-of-the-art rainfall products including models, satellite-based and ground-based observations are
117 intercompared with the new SM2RAIN-CCI data set. In particular, the two following products are considered as
118 benchmark:

119 GPCC-FDD, available at 1° spatial sampling during the period 1988-2013 (ground based data set) at daily temporal
120 resolution, used for calibrating SM2RAIN;

121 MSWEP, available from 1st January 1979 to 31st December 2015 at 0.25° spatial sampling on a daily basis (combination
122 of models, ground measurements and satellite observations), used as independent benchmark for the yearly global
123 analysis.

124 Three rainfall data sets are additionally used for cross-comparison with the SM2RAIN-CCI product:

- 125 1) TMPA 3B42RT (hereinafter referred to as TRMMRT), available from 1st March 2000 to present at 0.25°
126 spatial resolution for the $\pm 50^\circ$ latitude band every 3 hours (only satellite);
- 127 2) CMORPH raw data (hereinafter referred to as CMORPH), available from 1st January 2000 to present at 0.25°
128 spatial resolution for the $\pm 60^\circ$ latitude band every 3 hours (only satellite);
- 129 3) ERA-Interim reanalysis product, available from 1st January 1978 to present at 0.77° spatial sampling on a daily
130 basis (Dee et al., 2011) (reanalysis).

131 Due to the different spatial sampling and coverage (both in space and in time), the assessment is carried out during the
132 period 1998-2013 for the $\pm 50^\circ$ latitude band (due to data availability TRMMRT and CMORPH are considered starting
133 from 2000).

134 The GPCC-FDD data set is a gauge-based product. The number of stations used in the data set varies throughout the
135 years. In total, data from more than 60000 stations are used. GPCC-FDD is provided on a global scale over a grid with
136 1° spatial sampling and on a daily basis. The product is available for the period 1988-2013. Here, GPCC-FDD is used
137 as benchmark because it is completely independent from any satellite data and it does not contain any missing values
138 (Herold et al., 2017). For further details, the reader is referred to Schamm et al. (2015).

139 MSWEP is a recently developed rainfall data set that combines precipitation information from several sources,
140 including GPCC-FDD, TRMMRT, CMORPH and ERA-Interim. The estimates obtained through satellite sensors,
141 global models and in-situ stations are merged by the use of integration weights. The product is available from 1979 to
142 2015 with a spatial sampling of 0.25°. More information about MSWEP can be found in Beck et al. (2016).

143 TRMMRT provides rainfall estimates by taking advantage of multiple satellite sensors, i.e., the TRMM Microwave
144 Imager (TMI), the Special Sensor Microwave Imager (SSM/I), the Advanced Microwave Scanning Radiometer - Earth
145 Observing System (AMSR-E) and the Advanced Microwave Sounding Unit B (AMSU-B). The microwave estimates
146 are blended with infrared (IR) observations derived from sensors on board of Geostationary Earth Orbit (GEO)
147 platforms to obtain rainfall estimates at higher temporal and spatial resolution. The product is provided for the $\pm 50^\circ$
148 latitude band over a grid with a 0.25° spacing every 3 hours. Daily accumulated rainfall is computed by summing up all
149 rainfall estimates within one day. In this study the TMPA-3B42RT version 7 is used. For more details about the
150 TRMMRT product, the reader is referred to Huffman et al. (2007).

151 CMORPH uses precipitation estimates derived from the same microwave sensors used for TRMMRT generation, and
152 uses GEO-IR data to propagate the microwave estimates at the times between two successive microwave satellite



153 overpasses. The product is considered at daily temporal resolution over the 0.25° sampling TRMMRT grid for the ± 60°
154 latitude band. In this study, CMORPH raw data version 1.0 are considered. The reader is referred to Joyce et al. (2004)
155 for more details about CMORPH.

156 ERA-Interim is a reanalysis product provided by the European Centre for Medium-Range Weather Forecasts
157 (ECMWF). It is based on a global atmospheric model in which different types of observations are routinely assimilated.
158 The product is available from 1979 with a spatial resolution of about 0.77°. The data used have been downloaded from
159 the ECMWF FTP (<http://apps.ecmwf.int/datasets/data/interim-full-daily/levtype=sfc/>) resampled over the
160 0.25° CCI grid. For further details about ERA-Interim, the reader is referred to Dee et al. (2011).

161 2.1.2 ESA CCI Soil Moisture

162 The ESA CCI (<http://www.esa-soilmoisture-cci.org/>) provides long-term SM data sets for the period 1978-2015 (Liu et
163 al., 2011; Dorigo et al., 2015; Dorigo et al., in review). The products are provided on a global scale with a spatial
164 sampling of 0.25° with daily temporal sampling in three different configurations. The passive microwave product
165 (hereinafter referred to as “PASSIVE”) is provided for the period 1978-2015 and it is generated by merging SM
166 products derived from the Scanning Multichannel Microwave Radiometer (SMMR, operating at 6.6 and 10.7 GHz, Owe
167 et al., 2001), the Special Sensor Microwave Imager (SSM/I, operating at 19.35 GHz, Owe et al., 2008), the TRMM
168 Microwave Imager (TMI, operating at 10.65 GHz and above, Gao et al., 2006), the Advanced Microwave Scanning
169 Radiometer - Earth Observing System (AMSR-E, operating at 6.9 and 10.65 GHz, Owe et al. 2008) and its successor
170 AMSR2 (operating at 6.93, 7.3 and 10.65 GHz), WindSat (operating between 6.8 and 37 GHz, Li et al., 2010 and
171 Parinussa et al., 2012) and the ESA Soil Moisture and Ocean Salinity mission (SMOS, Kerr et al., 2012). Although the
172 PASSIVE data set is obtained by considering some of the sensors used for creating the TMPA products, this will not
173 impact the comparison between TRMMRT and SM2RAIN-CCI as different microwave frequency are taken into
174 account for rainfall estimation. The Active data set (hereinafter referred to as “ACTIVE”) is provided for the period
175 1991-2015 and it is generated by merging active microwave satellite retrievals from the European Remote Sensing
176 satellites (ERS-AMI, operating at 5.3 GHz) and from the Advanced Scatterometer (ASCAT, operating at 5.255 GHz,
177 Wagner et al., 2013) onboard the Metop-A and -B satellites. The third data set (hereinafter referred to as
178 “COMBINED”) is obtained by merging the ACTIVE and PASSIVE products. The merging of the individual data sets is
179 performed by means of a weighted averaging which is parameterized using a triple collocation (TC, Stoffelen, 1998)
180 approach (Gruber et al., accepted). In this study, we consider the ESA CCI SM product at version v03.2. For further
181 details regarding the ESA CCI SM product development, sensors availability and performances the reader is referred to
182 Liu et al., (2011; 2012), Dorigo et al., (2015; in review) and Wagner et al., (2012).

183 2.2 ESA CCI Soil Moisture pre-processing

184 Before applying SM2RAIN algorithm the following preprocessing steps are applied to the ESA CCI SM data sets. A
185 static mask (Figure 1) is used to mask out periods with high frozen soil and snow probability, rainforest areas and areas
186 with high topographic complexity. The latter two are provided within the ESA CCI SM data portal. Notice that deserts
187 are particularly challenging for SM retrieval from active instruments. Therefore, we use the passive data set only in
188 such areas (see Section 2.3), which typically provides more reliable retrievals over desert areas (Dorigo et al., 2010).
189 Moreover, a dynamic mask is applied to SSM data on a daily basis in order to remove observations characterized by
190 issues in the retrieval (frozen soil, dense vegetation). This mask is provided alongside with each of the ESA CCI SM
191 products. After the application of the dynamic mask, many temporal gaps are found within the SM time series. In order



192 to reduce the data gaps, the time series are interpolated to 00:00 UTC. A maximum data gap of three days is considered
 193 for the temporal interpolation. Data gaps larger than three days are left empty, i.e., no rainfall estimation is carried out
 194 within these intervals. Prior to 1998, the SM data sets are characterized by a low temporal coverage and a reduced data
 195 quality (Dorigo et al., 2015). Thus, the SM2RAIN-CCI product is generated only for the period 1998-2015. The original
 196 ACTIVE and PASSIVE CCI SM data sets have been read and preprocessed by using routines developed in Python@
 197 language by the TUWIEN Remote Sensing Research Group (Ciabatta et al., 2016). After the preprocessing steps, the
 198 ESA CCI SM data are ready to be used as input in SM2RAIN.

199 2.3 SM2RAIN algorithm and SM2RAIN-CCI rainfall product generation

200 The SM2RAIN algorithm (Brocca et al., 2013, 2014) allows to derive rainfall estimates from SM observations. It is
 201 based on the inversion on the following soil water balance equation:

$$202 \quad p(t) = Z^* ds(t) / dt + as(t)^b \quad (1)$$

203 where $p(t)$ is the estimated rainfall, Z^* is the soil water capacity (soil depth times soil porosity), $s(t)$ is the relative soil
 204 saturation, t is the time and a and b are two parameters describing the non-linearity between soil saturation and
 205 drainage. Z^* , a and b are estimated through calibration. The algorithm is based on the assumption that during rainfall
 206 evapotranspiration is negligible and surface runoff occurs only when the soil is fully saturated (Brocca et al., 2015).
 207 SM2RAIN has also the main limitation of not being able to estimate rainfall if the soil is close to saturation, since no
 208 SM variations can be observed after rainfall events in such conditions.

209 The algorithm has proved to accurately estimate rainfall both on a regional (Abera et al., 2016; Brocca et al., 2013;
 210 2015; 2016; Ciabatta et al., 2015, 2017) and on a global scale (Brocca et al., 2014; Koster et al., 2016). For further
 211 details about the SM2RAIN formulation, the reader is referred to Brocca et al. (2013; 2014).

212 The SM2RAIN parameters are obtained by minimizing the Root Mean Square Difference (RMSD) between the 5-day
 213 estimated rainfall and the GPCC-FDD data during three calibration periods 1998-2001, 2002-2006, 2007-2013 on a
 214 pixel-by-pixel basis. We considered 5-day of accumulation to reduce the amount of data and speed-up the calibration
 215 step. The use of different calibration periods relies on the different data and sensors that we used for building the
 216 ACTIVE and PASSIVE SSM data sets (Table 1, see also Dorigo et al., 2012). The calibration is performed on a pixel-
 217 by-pixel basis separately for ACTIVE and PASSIVE. SM2RAIN was also applied to the COMBINED SSM data set,
 218 but we observed a reduction of performance with respect to the individual ACTIVE and PASSIVE products (not
 219 shown), hence the COMBINED SSM data set is not considered here. In order to match the different spatial resolutions
 220 of the considered data sets, GPCC-FDD was regridded to the 0.25° CCI grid by using the *griddata* function
 221 implemented in MATLAB® R2012a, through linear interpolation. After the application of SM2RAIN to the ACTIVE
 222 and PASSIVE SM data sets, the two obtained rainfall products are integrated through:

$$223 \quad P_{SM2RAIN-CCI} = kP_{ACT} + (1-k)P_{PAS} \quad (2)$$

224 where P_{ACT} and P_{PAS} are the two rainfall data sets obtained through the application of SM2RAIN to the ACTIVE and the
 225 PASSIVE SM data sets, respectively, and $P_{SM2RAIN-CCI}$ is the final SM2RAIN-CCI rainfall data set. The integration
 226 weights (k) are estimated through (Kim et al., 2015):

$$227 \quad k = \frac{\rho_{AB} - \rho_{AP} * \rho_{AB}}{\rho_{PB} - \rho_{AP} * \rho_{AB} + \rho_{AB} - \rho_{AP} * \rho_{PB}} \quad (3)$$

228 Where ρ is the Pearson correlation coefficient between two data sets with the subscript A, P and B denoting the
 229 ACTIVE, the PASSIVE and the benchmark (GPCC-FDD in this case) rainfall estimates, respectively. When one of the



230 two data sets (P_{ACT} or P_{PAS}) is not available at a certain location (e.g., due to unfavorable retrieval conditions), then only
231 the available one is used for the generation of the combined rainfall product. The workflow is depicted in Figure 2. The
232 data are available in netCDF format via the CCI SM FTP server. The rainfall data are provided in mm per day, over
233 land at 0.25° of sampling. The SM2RAIN-CCI data set temporal coverage will be extended when new ESA CCI SM
234 updates will be released.

235 3 SM2RAIN-CCI performance

236 The SM2RAIN-CCI rainfall data set is available from 1st of January 1998 to 31st December 2015 with daily temporal
237 resolution. The data are provided over a 0.25° grid on a global scale, given the native spatial resolution of SM
238 observation of 25 and 50 km. The spatio-temporal coverage is reported in Figure 3. As it can be seen, there is an
239 increase of available data after 2002 and 2007, corresponding to the start of the AMSR-E and ASCAT operations,
240 respectively. Before 2002, the ESA CCI SM products are characterized by a small amount of data, due to longer revisit
241 times of the used satellites. Before that date, the rainfall estimates obtained through SM2RAIN should be used with
242 caution because of the likelihood of missing precipitation events. The lack of data over tropical areas and at high
243 latitudes is due to the application of the mask described above. Figure 3 also shows the mean daily rainfall for the
244 SM2RAIN-CCI data set during the analysis period. As it can be seen, an increase in the daily values can be observed
245 after 2007, especially over the tropical areas, where the seasonality is well reproduced, due to the higher number of
246 satellite overpasses.

247 When compared to the GPCC-FDD rainfall data set, SM2RAIN-CCI shows relatively good performance for 5-day
248 rainfall accumulation both in terms of correlation and RMSD, as drawn in Figure 4 for the $\pm 50^\circ$ latitude bands during
249 the three calibration periods at 1° of spatial resolution, in order to perform a fair comparison with the benchmark.
250 SM2RAIN-CCI rainfall shows relatively good agreement with GPCC-FDD, especially over Africa, Australia, India and
251 South America in terms of correlation (R). The RMSD pattern is related to the rainfall regimes. The highest values are
252 located in those regions characterized by high total annual precipitation, e.g. tropical areas. The comparison also
253 provides better performance for the 2007-2013 period than for the 1998-2001 and 2002-2006 periods due to the better
254 temporal coverage of the ESA CCI SM products and their improved accuracy (Dorigo et al., 2015). As it can be seen in
255 Figure 4, the median R (RMSD) obtained for the 1998-2001 calibration period is 0.54 (10.94 mm), while for the 2007-
256 2013 period, a median value of 0.65 (9.6 mm) is obtained. Indeed, due to the nature of the SM2RAIN algorithm, more
257 frequent satellite overpasses are expected to provide more reliable rainfall estimates. SM2RAIN-CCI shows a lower
258 performance over the Sahara Desert and at high latitudes, due to lower SM data quality over these regions. Figure 4 also
259 displays the lower performances obtained for the eastern US. A similar performance pattern was also found by Massari
260 et al. (2017) who calculated global correlation of different rainfall data sets by applying the Extended TC (McColl et
261 al. 2014) analysis. A cross-comparison of SM2RAIN-CCI with GPCC, TRMM, CMORPH, ERA-Interim and MSWEP
262 is reported in Figure 5. The Figure displays the $1^\circ \times 1^\circ$ ($\pm 50^\circ$) correlation maps of 5 day of accumulated rainfall (on the
263 left) and the differences in the mean annual rainfall (on the right) between SM2RAIN-CCI and the other rainfall data
264 sets. The difference in the mean annual rainfall are calculated by subtracting the mean annual rainfall of each data set to
265 the one provided by SM2RAIN-CCI. The analysis shows that SM2RAIN-CCI rainfall estimates are in good agreement
266 with the state-of-the-art data sets both in terms of R and mean annual rainfall. Non-negligible differences can be
267 observed over the Sahara Desert, Eastern US, South America, the tropical area and over Europe, where SM2RAIN-CCI



268 provides a smaller amount of rainfall than the other rainfall data sets. On the other hand, very good performance can be
269 observed over Africa, Brazil, western US, India and Australia, both in terms of R and mean annual rainfall.
270 Seven macro-regions worldwide have been selected to check the capability of the SM2RAIN-CCI in estimating rainfall
271 under different climatic conditions. Therefore, Mean monthly rainfall (MMR) was computed from GPCC-FDD and
272 SM2RAIN-CCI during the period 1998-2013 within these regions, illustrated as green boxes in Figure 6. From Figure
273 6, one can see that the temporal rainfall patterns agree well in all considered macro-regions. SM2RAIN-CCI provides a
274 general underestimation before 2007, due to the increased number of data gaps. Indeed, if the GPCC-FDD MMR is
275 estimated only when SM observations are available (i.e. when both GPCC-FDD and SM2RAIN-CCI provide a rainfall
276 estimate), the two estimates are very close to each other, for the entire analysis period.

277 3.1 SM2RAIN-CCI performance over time

278 Figure 7 shows box plots of R and RMSD values between SM2RAIN-CCI and MSWEP on a yearly scale. The use of
279 an independent benchmark removes the effect of the algorithm calibration against GPCC-FDD data set and (partly) the
280 effect of in situ stations density on the benchmark reliability. The comparison is carried out over the $\pm 50^\circ$ latitude band.
281 The SM2RAIN-CCI rainfall product generally agrees well with MSWEP. An increasing trend in the performance can
282 be observed over time during the analysis period, highlighting the impact of data availability on estimation uncertainty.
283 The most significant improvements can be observed in 2003 and 2007, corresponding to the start of AMSR-E and
284 ASCAT operations, respectively. Figure 7 shows that the SM2RAIN-CCI product provides the lowest R (0.57) during
285 2001 and the highest (0.80) during 2013. Similar patterns are found for the RMSD score. The improvements are not just
286 recognizable in the median values, but also in the spread of R and RMSD values within each year.

287 3.2 Regional scale assessment

288 For the regional scale assessment, three macro-areas with a high rain gauge station density are selected, which are
289 Europe, India, and Australia. SM2RAIN-CCI estimates are compared against data from these ground-based
290 measurements on the 0.25° scale.

291 The comparison over Europe is carried out by considering the so-called E-OBS rainfall data set (Haylock et al., 2008)
292 as benchmark. This data set provides daily rainfall estimates over the European area at 0.25° spatial resolution starting
293 from 1950. The estimates are obtained by interpolating via a three-step kriging procedure rainfall values from gauge
294 stations over Europe. For this analysis, we consider the region between -9.875°W and 24.875°E longitude and between
295 28.125°N and 59.875°N latitude. Due to the TRMM orbit geometry, the considered TRMMRT data set covers only the
296 area between 28.125°N and 49.875°N latitude. The analysis is carried out during the period 2002-2015, in order to
297 avoid to consider partly the data calibrated during the period 1998-2001. Figure 8 shows R and RMSD statistics against
298 E-OBS for 5 days accumulated rainfall. As can be seen, SM2RAIN-CCI provides a median R lower than 0.5, close to
299 that provided by TRMMRT and CMORPH. All rainfall products show a large variability in terms of R, ranging
300 between -0.4 and almost 1. In terms of RMSD, all the products show median values close to 10 mm, with values
301 ranging approximately between 5 and 20 mm. ERA Interim provided very good performance, both in terms of R and
302 RMSD, due to the use of dense meteorological networks in Europe that guarantees good performance of the ERA-
303 Interim reanalysis product. It is worth noting that ERA-Interim does not use raingaug data, but only other
304 meteorological variables. MSWEP provided the best performance over Europe, due to the merging of different rainfall
305 products. In general, SM2RAIN-CCI performs quite well in southern Europe (Italy, Spain and southern France). In



306 central and northern Europe, observations are subject to a high selective masking of frozen soil and snow, which
307 reduces the temporal observation density and hence also the SM2RAIN retrieval accuracy.

308 The analysis over India is carried out during the period 2002-2015 using observed rainfall data provided by the India
309 Meteorological Department (IMD). The considered region spans from 70°E to 90°E longitude and from 5°N to 25°N
310 latitude. As can be seen in Figure 8, R values are generally higher than those obtained over Europe, most likely due to
311 the strong seasonal signal. The SM2RAIN-CCI data set shows a median R of 0.60, which is slightly lower than that
312 achieved by TRMMRT, CMORPH, ERA Interim and MSWEP. In terms of RMSD, values are generally higher than
313 over Europe, which result from the larger annual precipitation amount. SM2RAIN-CCI performs very well over India,
314 and is less reliable along the coast and in the Northern parts of the country due to the impact of the Himalaya.

315 Over Australia, the Australian Water Availability Project (AWAP) observed rainfall data during the period 2010-2013
316 is used as benchmark. The analysis box spans from 120°E to 160°E longitude and from 10°S to 40°S latitude. The
317 analysis shows very good results both in terms of R and RMSD (Figure 8). SM2RAIN-CCI provides a median R of 0.71
318 which is higher than that obtained with TRMMRT and CMORPH. Moreover, R values are consistently higher than 0.5
319 in the entire macro-region. In terms of RMSD, median value of 11.90 mm is obtained for SM2RAIN-CCI, while
320 TRMMRT and CMORPH provided median values of 16.56 mm and 13.52 mm, respectively. The large variability of
321 errors is related to the different rainfall regimes in Australia, i.e. tropical climate in the northern sector and drier
322 conditions in the inland part. In tropical rainfall regimes, the SM2RAIN algorithm is often subject to close-to-saturation
323 soil conditions, which lead to a general underestimation of precipitation. Results are consistent with those of Tarpanelli
324 et al., (2017) who applied the SM2RAIN algorithm to multiple satellite SM products over India.

325 4 CONCLUSIONS

326 This study presents a new rainfall data set obtained through the application of the SM2RAIN algorithm (Brocca et al.,
327 2014) to the ACTIVE and the PASSIVE ESA CCI SM products (Dorigo et al., 2017, in review) during the period 1998-
328 2015, named SM2RAIN-CCI. The algorithm is calibrated using the GPCC-FDD data set. Due to the different
329 characteristics of the satellite sensors used for creating the input SM data sets, three different calibrations periods are
330 considered: 1) 1998-2001; 2) 2002-2006 and 3) 2007-2013. The minimization of the RMSD between 5-day
331 accumulated rainfall from GPCC-FDD and SM2RAIN applied to both the ACTIVE and PASSIVE ESA CCI SM data
332 sets is used as objective function. After the calibration, the two rainfall products derived from the ACTIVE and the
333 PASSIVE ESA CCI SM data sets are merged into the final SM2RAIN-CCI data set. SM2RAIN-CCI data set is
334 available on a global scale (over land) with a daily temporal sampling on a 0.25° regular grid. A mask is applied to the
335 data set in order to remove pixels and observations characterized by high topographic complexity, frozen soil and high
336 snow probability.

337 The SM2RAIN-CCI data set is compared to 3 different global (or quasi-global) state-of-the-art rainfall products in order
338 to check its capability in rainfall estimation. In general, the SM2RAIN-CCI shows relatively good performance in
339 precipitation estimation, especially during the 2007-2013 period (see Figure 4 and 5). On a global scale and for the
340 entire analysis period, 5-day SM2RAIN-CCI rainfall estimates provide a median R of 0.67 when compared to MSWEP
341 (see Figure 7).

342 The product is further evaluated over three macro-areas (Europe, India and Australia) where it provides satisfactory
343 results, both in terms of R and RMSD when compared to spatially interpolated high-density rain gauge measurement
344 networks (see Figure 8). Higher errors are found over India and Australia due to the larger total rainfall amounts of



345 precipitation. However, the analysis showed relatively good results also over 5 other considered macro-regions (see
346 Figure 5) when compared to GPCC-FDD. In these regions, the impact of reduced temporal coverage on retrieval
347 accuracy is clearly visible.

348 The multi-sensor data sets provided by ESA CCI and the application of SM2RAIN could open new perspectives and
349 opportunities in the use of satellite rainfall products over developing countries or in remote areas with non-existing or
350 spatially-sparse ground monitoring networks. The new product is potentially suitable for several applications in the
351 domains of climate (due to the long temporal coverage) and hydrology (due to good capabilities in accumulated rainfall
352 estimation), complementing other state-of-the-art rainfall products. Moreover, the SM2RAIN-CCI is completely
353 independent from other existing state-of-the-art precipitation products, therefore offering an additional long-term data
354 set that can be used for independently evaluating these global-scale precipitation products as shown by Massari et al.
355 (2017).

356 ACKNOWLEDGEMENT

357 The authors gratefully acknowledge the E-OBS data set from the EU-FP6 project ENSEMBLES (<http://ensembles-eu.metoffice.com>) and the data providers in the ECA&D project (<http://www.ecad.eu>). This work is supported by
358 the ESA Climate Change Initiative (CCI, <http://www.esa-soilmoisture-cci.org/>, Contract No.
359 [400011226/14/I-NB](http://www.esa-soilmoisture-cci.org/)) and the earth2Observe project (European Union's Seventh Framework Programme, Grant
360 Agreement No. 603608).

362 REFERENCES

- 363 Abera, W., Brocca, L., Rigon, R. (2016). Comparative evaluation of different satellite rainfall estimation products and
364 bias correction in the Upper Blue Nile (UBN) basin. *Atmospheric Research*, 178-179, 471-483.
- 365 Ashouri, H., Hsu, K.L., Sorooshian, S., Braithwaite, D.K., Knapp, K.R., Cecil, L.D., Nelson, B.R., Prat, O.P. (2015).
366 PERSIANN-CDR: Daily Precipitation Climate Data Record from Multisatellite Observations for Hydrological and
367 Climate Studies. *Bull. Amer. Meteor. Soc.*, 96, 6983. Doi: <http://dx.doi.org/10.1175/BAMS-D-13-00068.1>
- 368 Beck, H.E., van Dijk, A.I.J.M., Levizzani, V., Schellekens, J., Miralles, D.G., Martens, B., de Roo, A. (2016). MSWEP: 3-
369 hourly 0.25° global gridded precipitation (1979–2015) by merging gauge, satellite, and reanalysis data, *Hydrology and*
370 *Earth System Sciences*, 21, 589–615, doi:10.5194/hess-21–589-2017, 2017.
- 371 Brocca, L., Melone, F., Moramarco, T., Wagner, W. (2013). A new method for rainfall estimation through soil moisture
372 observations. *Geophys. Res. Lett.*, 40(5), 853-858.
- 373 Brocca, L., Ciabatta, L., Massari, C., Moramarco, T., Hahn, S., Hasenauer, S., Kidd, R., Dorigo, W., Wagner, W., Levizzani,
374 V. (2014). Soil as a natural raingauge: estimating rainfall from global satellite soil moisture data. *J. Geophys. Res.*,
375 119(9), 5128–5141.
- 376 Brocca, L., Massari, C., Ciabatta, L., Moramarco, T., Penna, D., Zuecco, G., Pianezzola, L., Borga, M., Matgen, P.,
377 Martínez-Fernández, J. (2015). Rainfall estimation from in situ soil moisture observations at several sites in Europe: an
378 evaluation of SM2RAIN algorithm. *Journal of Hydrology and Hydromechanics*, 65, 3, 201-209.



- 379 Brocca, L., Pellarin, T., Crow, W.D., Ciabatta, L., Massari, C., Ryu, D., Su, C.H., Rüdiger, C., Kerr, Y. (2016), Rainfall
380 estimation by inverting SMOS soil moisture estimates: A comparison of different methods over Australia, *J. Geophys.*
381 *Res. Atmos.*, 121, doi:10.1002/2016JD025382.
- 382 Ciabatta, L., Brocca, L., Massari, C., Moramarco, T., Gabellani, S., Puca, S., Rinollo, A., Wagner, W. (2015).
383 Integration of satellite soil moisture and rainfall observations over the Italian territory. *Journal of Hydrometeorology*,
384 16(3), 1341-1355.
- 385 Ciabatta, L., Massari, C., **Brocca, L.**, Reimer, C., Hann, S., Paulik, C., Dorigo, W., Wagner, W. (2016) Using Python®
386 language for the validation of the CCI soil moisture products via SM2RAIN. *PeerJ Preprints*, 4:e2131v2,
387 doi:10.7287/peerj.preprints.2131v2
- 388 Ciabatta, L., Marra, A.C., Panegrossi, G., Casella, D., Sanò, P., Dietrich, S., Massari, C., Brocca, L. (2017). Daily
389 precipitation estimation through different microwave sensors: verification study over Italy. *Journal of Hydrology*,
390 545:436-450.
- 391 Crow, W.T., Huffman, G.F., Bindlish, R., Jackson, T.J. (2009). Improving satellite rainfall accumulation estimates using
392 spaceborne soil moisture retrievals. *J. Hydrometeorol.*, 10, 199- 212.
- 393 Crow, W.T., Van Den Berg, M.J., Huffman, G.J., Pellarin, T. (2011). Correcting rainfall using satellite-based surface soil
394 moisture retrievals: The Soil Moisture Analysis Rainfall Tool (SMART). *Water Resources Research*, 47 (8).
- 395 Dee, D.P., Uppala, S.M., Simmons, A.J., Berrisford, P., Poli, P., Kobayashi, S., Andrae, U., Balmaseda, M.A., Balsamo, G.,
396 Bauer, P., Bechtold, P., Beljaars, A.C.M., van de Berg, L., Bidlot, J., Bormann, N., Delsol, C., Dragani, R., Fuentes, M.,
397 Geer, A.J., Haimberger, L., Healy, S.B., Hersbach, H., Holm, E.V., Isaksen, I., Kallberg, P., Kohler, M., Matricardi, M.,
398 McNally, A.P., Monge-Sanz, B.M., Morcrette, J.J., Park, B.K., Peubey, C., de Rosnay, P., Tavolato, C., Thepaut, J.N.,
399 Vitard, F. (2011). The ERA-Interim reanalysis: configuration and performance of the data assimilation system. *Quarterly*
400 *Journal of the Royal Meteorological Society*, 137 (656A): 553-597.
- 401 Dinku, T., P. Ceccato, E. Grover-Kopec, M. Lemma, S.J. Connor, C.F. Ropelewsky, 2007. Validation of satellite rainfall
402 products over East Africa's complex topography. *Int. J. Remote Sens.*, 28 (7), 1503–1526.
- 403 Dorigo, W.A., Scipal, K., Parinussa, R.M., Liu, Y.Y., Wagner, W., de Jeu, R.A.M., Naeimi, V. (2010). Error characterisation
404 of global active and passive microwave soil moisture datasets. *Hydrology and Earth System Sciences*, 14-12, 2605-
405 2616.
- 406 Dorigo, W. A., R. A.M. de Jeu, D. Chung, R. M. Parinussa, Y. Y. Liu, W. Wagner, and D. Fernandez-Prieto (2012),
407 Evaluating global trends (1988-2010) in harmonized multi-satellite surface soil moisture, *Geophys. Res. Lett.*, VOL. 39,
408 L18405, 7 PP. 2012 doi:10.1029/2012GL052988.
- 409 Dorigo, W.A., Gruber, A., De Jeu, R.A.M., Wagner, W., Stacke, T., Loew, A., Albergel, C., Brocca, L., Chung, D.,
410 Parinussa, R.M., Kidd, R. (2015). Evaluation of the ESA CCI soil moisture product using ground-based observations.
411 *Remote Sensing of Environment*, doi: 10.1016/j.rse.2014.07.023.
- 412 Dorigo, W.A., Wagner, W., Albergel, C., Abrecht, F., Balsamo, G., Brocca, L., Chung, D., Ertl, M., Forkel, M.,
413 Gruber, A., Haas, E., Hamer, P., Hirschi, M., Ikonen, J., de Jeu, R., Kidd, R., Lahoz, W., Liu, Y.Y., Miralles, D.,
414 Mistelbauer, T., Nicolai-Shaw, N., Parinussa, R., Pratola, C., Reimer, C., van der Schalie, R., Seneviratne, S.I.,
415 Smolander, T., Lecomte, P.. (in review). ESA CCI Soil Moisture for improved Earth system understating: state-of-the-
416 art and future decision. Submitted to *Remote Sensing of Environment*.



- 417 Funk, C., Peterson, P., Landsfeld, M., Pedreros, D., Verdin, J., Shukla, S., Husak, G., Rowland, J., Harrison, L., Hoell, A.,
418 Michaelsen, J. (2015). The climate hazards infrared precipitation with stations—a new environmental record for
419 monitoring extremes. *Scientific Data* 2, 150066. doi:10.1038/sdata.2015.66 2015.
- 420 Gao, H., Wood, E. F., Jackson, T. J., Drusch, M., and Bindlish, R., 2006: Using TRMM/TMI to retrieve surface soil
421 moisture over the southern United States from 1998 to 2002. *J. Hydrometeorology*, 7(1), 23-38, DOI:
422 10.1175/JHM473.1
- 423 Gruber, A., Dorigo, W. Crow, W., Wagner, W. (accepted). Triple collocation based merging of satellite soil moisture
424 retrievals". *IEEE Transactions on Geoscience and Remote Sensing*.
- 425 Haylock, M.R., N. Hofstra, A.M.G. Klein Tank, E.J. Klok, P.D. Jones, M. New. 2008: A European daily high-
426 resolution gridded dataset of surface temperature and precipitation. *J. Geophys. Res (Atmospheres)*, 113, D20119,
427 doi:10.1029/2008JD10201
- 428 Herold, N., Behrangi, A., Alexander, L., V. (2017). Large uncertainties in observed daily precipitation extremes over
429 land. *Journal of Geophysical Research (Atmospheres)*, 122-2, 668-981.
- 430 Hou, A.Y., Kakar, R.K., Neeck, S., Azarbarzin, A.A., Kummerow, C.D., Kojima, M., Oki, R., Nakamura, K., Iguchi, T.
431 (2014). The Global Precipitation Measurement (GPM) mission. *Bull. Amer. Meteor. Soc.*, 95(5), 701-722.
- 432 Hsu, K., Gao, X., Sorooshian, S., Gupta, H.V. (1997). Precipitation Estimation from Remotely Sensed Information
433 Using Artificial Neural Networks, *Journal of Applied Meteorology*, Vol. 36, No. 9, 1176-1190.
- 434 Huffman, G.J., Adler, R.F., Bolvin, D.T., Gu, G., Nelkin, E.J., Bowman, K.P., Hong, Y., Stocker, E.F., Wolff, D.B.
435 (2007). The TRMM Multisatellite Precipitation Analysis (TMPA): Quasi global, multiyear, combined-sensor
436 precipitation estimates at fine scales. *J. Hydrometeor.*, 8(1), 38-55.
- 437 Joyce R. J., Janowiak J. E., Arkin P. A., Xie P. (2004). CMORPH: A method that produces global precipitation
438 estimates from passive microwave and infrared data at high spatial and temporal resolution, *J. Hydrometeorol.*, 5(3),
439 487–503.
- 440 Kerr, Y.H., Waldteufel, P., Richaume, P., Wigneron, J.-P., Ferrazzoli, P., Mahmoodi, A., Al Bitar, A., Cabot, F.,
441 Gruhier, C., Juglea, S.E., Leroux, D., Mialon, A., Delwart, S. (2012). The SMOS Soil Moisture Retrieval Algorithm.
442 *IEEE Trans. Geosci. Remote Sens.*, 50(5), 1384-1403.
- 443 Kidd C., Matsui T., Chern J., Mohr K., Kummerow C. D., and Randel D. (2016). Global precipitation estimates from
444 cross-track passive microwave observations using a physically based retrieval scheme, *J. Hydrometeorol.*, 17(1), 383–
445 400.
- 446 Kim, S., Parinussa, R. M., Liu, Y. Y., Johnson, F. M., Sharma, A. (2015). A framework for combining multiple soil
447 moisture retrievals based on maximizing temporal correlation. *Geophysical Research Letters*, 42(16), 6662-6670.
- 448 Koster, R.D., Brocca, L., Crow, W.T., Burgin, M.S., De Lannoy, G.J.M. (2016). Precipitation Estimation Using L-Band
449 and C-Band Soil Moisture Retrievals. submitted to *Water Resources Research*. *Water Resour. Res.*, 52,
450 doi:10.1002/2016WR019024.
- 451 Kucera, P.A., E.E. Ebert, F.J. Turk, V. Levizzani, D. Kirschbaum, F.J. Tapiador, A. Loew, M. Borsche, 2013.
452 Precipitation from space: Advancing earth system science. *Bull. Amer. Meteor. Soc.*, 94, 365-375.
- 453 Li, L., Gaiser, P.W., Gao, B.C., Bevilacqua, R.M., Jackson, T.J., Njoku, E.G., Rudiger, C., Calvet, J.C., Bindlish, R.
454 (2010). WindSat global soil moisture retrieval and validation. *IEEE Transactions on Geoscience and Remote Sensing*,
455 48 (5), 2224-2241.



- 456 Liu, Y. Y., Parinussa, R. M., Dorigo, W. A., De Jeu, R. A. M., Wagner, W., van Dijk, A. I. J. M., McCabe, M. F.,
457 Evans, J. P. (2011). Developing an improved soil moisture dataset by blending passive and active microwave satellite-
458 based retrievals. *Hydrology and Earth System Sciences*, 15, 425–436, doi:10.5194/hess-15-425-2011.
- 459 Liu, Y.Y., Dorigo, W.A., Parinussa, R.M., de Jeu, R.A.M., Wagner, W., McCabe, M.F., Evans, J.P., van Dijk, A.I.J.M.
460 (2012). Trend-preserving blending of passive and active microwave soil moisture retrievals, *Remote Sensing of*
461 *Environment*, 123, 280–297, doi: 10.1016/j.rse.2012.03.014.
- 462 Massari, C., Crow, W.D., Brocca, L., (2017). An assessment of the accuracy of global precipitation estimates without
463 gauge observations. *Hydrol. Earth Science Discuss.*, doi:10.5194/hess-2017-163, 2017.
- 464 McColl, K. A., Vogelzang, J., Konings, A. G., Entekhabi, D., Piles, M., & Stoffelen, A. (2014). Extended triple collocation:
465 Estimating errors and correlation coefficients with respect to an unknown target. *Geophysical Research Letters*,
466 41(17), 6229–6236. <https://doi.org/10.1002/2014GL061322>.
- 467 Owe, M., de Jeu, R.A.M., Walker, J. (2001). A methodology for surface soil moisture and vegetation optical depth
468 retrieval using the microwave polarization difference index, *IEEE Trans. Geosci. Remote Sens.*, 39, 1643–1694.
- 469 Owe, M., De Jeu, R.A.M., Holmes, T.R.H. (2008). Multi-sensor historical climatology of satellite derived global land
470 surface moisture. *J. Geophys. Res.*, 113, F01002.
- 471 Panegrossi, G., Casella, D., Dietrich, S., Marra, A.C., Petracca, M., Sanò, P., Mugnai, A., Baldini, L., Roberto, N.,
472 Adirosi, E., Cremonini, R., Bechini, R., Vulpiani, G., Porcù, F. (2016). Use of the GPM constellation for monitoring
473 heavy precipitation events over the Mediterranean region. *IEEE Trans. Geosci. Remote Sens.*, in press, doi:900
474 10.1109/JSTARS.2016.2520660.
- 475 Parinussa, R., Holmes, T.R.H., de Jeu, R. (2012). Soil moisture retrievals from the Windsat spaceborne polarimetric
476 microwave radiometer. *IEEE Transactions on Geoscience and Remote Sensing* 50(7): 2683–2694.
- 477 Pellarin, T., Louvet, S., Gruhier, C., Quantin, G., Legout, C. (2013). A simple and effective method for correcting soil
478 moisture and precipitation estimates using AMSR-E measurements. *Remote Sens. Environ.*, 136, 28–36.
- 479 Schamm, K., Ziese, M., Raykova, K., Becker, A., Finger, P., Meyer-Christoffer, A., Schneider, U. (2015). GPCP Full Data
480 Daily Version 1.0 at 1.0°: Daily Land-Surface Precipitation from Rain-Gauges built on GTS-based and Historic Data. DOI:
481 10.5676/DWD_GPCP/FD_D_V1_100.
- 482 Stoffelen, A. (1998): Toward the true near-surface wind speed: Error modeling and calibration using triple collocation,
483 *Journal of Geophysical Research*, 103, 7755, doi:10.1029/97JC03180.
- 484 Tarpanelli A., Massari C., Ciabatta L., Filippucci P., Amarnath G., Brocca L. (...) Exploiting a constellation of satellite
485 soil moisture sensors for accurate rainfall estimation. Submitted to *Advances in Water Resources*.
- 486 Trenberth, K.E., Asrar, G.R., 2014. Challenges and opportunities in water cycle research: WCRP contributions. *Surv.*
487 *Geophys.* 35(3), 515–532. doi:10.1007/s10712-012-9214-y.
- 488 Villarini, G., Mandapaka, P. V., Krajewski, W. F., and Moore, R. J.: Rainfall and sampling uncertainties: A rain gauge
489 perspective, *Journal of Geophysical Research*, 113, D11 102, doi:10.1029/2007JD009214,
490 <http://doi.wiley.com/10.1029/2007JD009214>, 2008.
- 491 Wagner, W., Dorigo, W., de Jeu, R., Fernandez, D., Benveniste, J., Haas, E., Ertl, M. (2012). Fusion of active and
492 passive microwave observations to create an Essential Climate Variable data record on soil moisture, *ISPRS Annals of*
493 *the Photogrammetry, Remote Sensing and Spatial Information Sciences (ISPRS Annals)*, Volume I-7, XXII ISPRS
494 Congress, Melbourne, Australia, 25 August–1 September 2012, 315–321.
- 495 Wagner, W., Hahn, S., Kidd, R., Melzer, T., Bartalis, Z., Hasenauer, S., Figa, J., de Rosnay, P., Jann, A., Schneider, S.,
496 Komma, J., Kubu, G., Bruggen, K., Aubrecht, C., Zuger, J., Gangkofner, U., Kienberger, S., Brocca, L., Wang, Y.,



- 497 Bloeschl, G., Eitzinger, J., Steinnocher, K., Zeil, P., Rubel, F. (2013). The ASCAT soil moisture product:
498 Specifications, validation results, and emerging applications. *Meteorologische Zeitschrift*, 22(1), 5-33.
- 499 Wanders, N., Pan, M., Wood, E.F. (2015). Correction of real-time satellite precipitation with multi-sensor satellite
500 observations of land surface variables. *Remote Sensing of Environment*, 160, 206-221.
- 501 Zhan, W., Pan, M., Wanders, N., Wood, E.F. (2015). Correction of real-time satellite precipitation with satellite soil
502 moisture observations. *Hydrol. Earth Syst. Sci.*, 19, 4275-4291.
- 503



504 **TABLES**

505

Sensor (Active/Passive)	Temporal interval
AMI-WS / SSMI & TMI	1998-01-01 to 2002-06-30
AMI-WS / AMSR-E	2002-07-01 to 2006-12-31
ASCAT-A & ASCAT B / AMSR-E & Windsat & SMOS & AMSR2	2007-01-01 to 2013-12-31
AMI-WS / SSMI & TMI & AMSR-E	1992-01-01 to 2006-12-31
ASCAT-A & ASCAT-B / AMSR-E & Windsat & SMOS & AMSR2	2007-01-01 to 2013-12-31

506

507 **Table 1 – Available sensors and temporal intervals considered for the SM2RAIN algorithm application.**

508

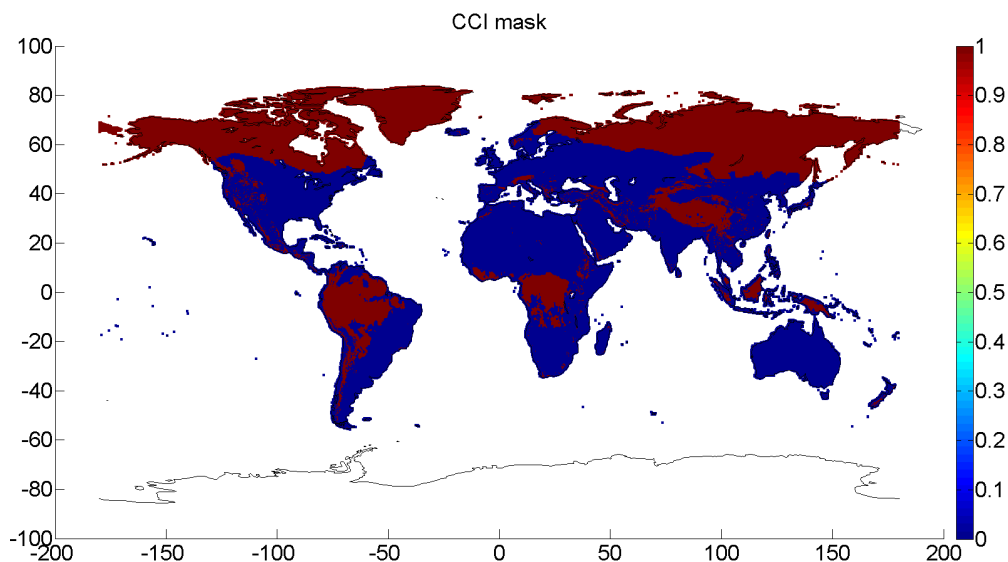
509

510

511

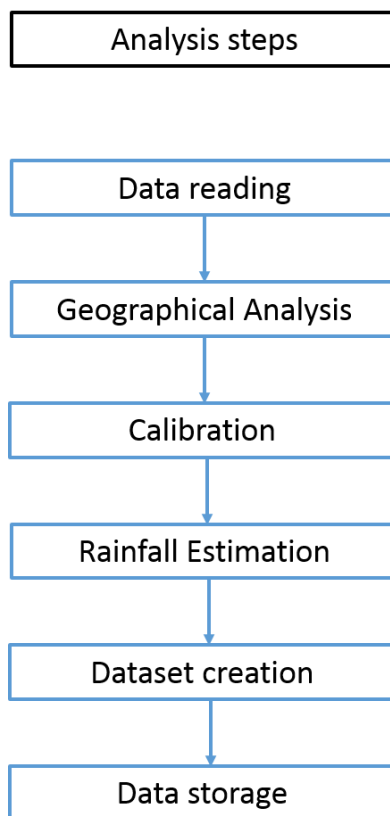


512 **FIGURES**



513

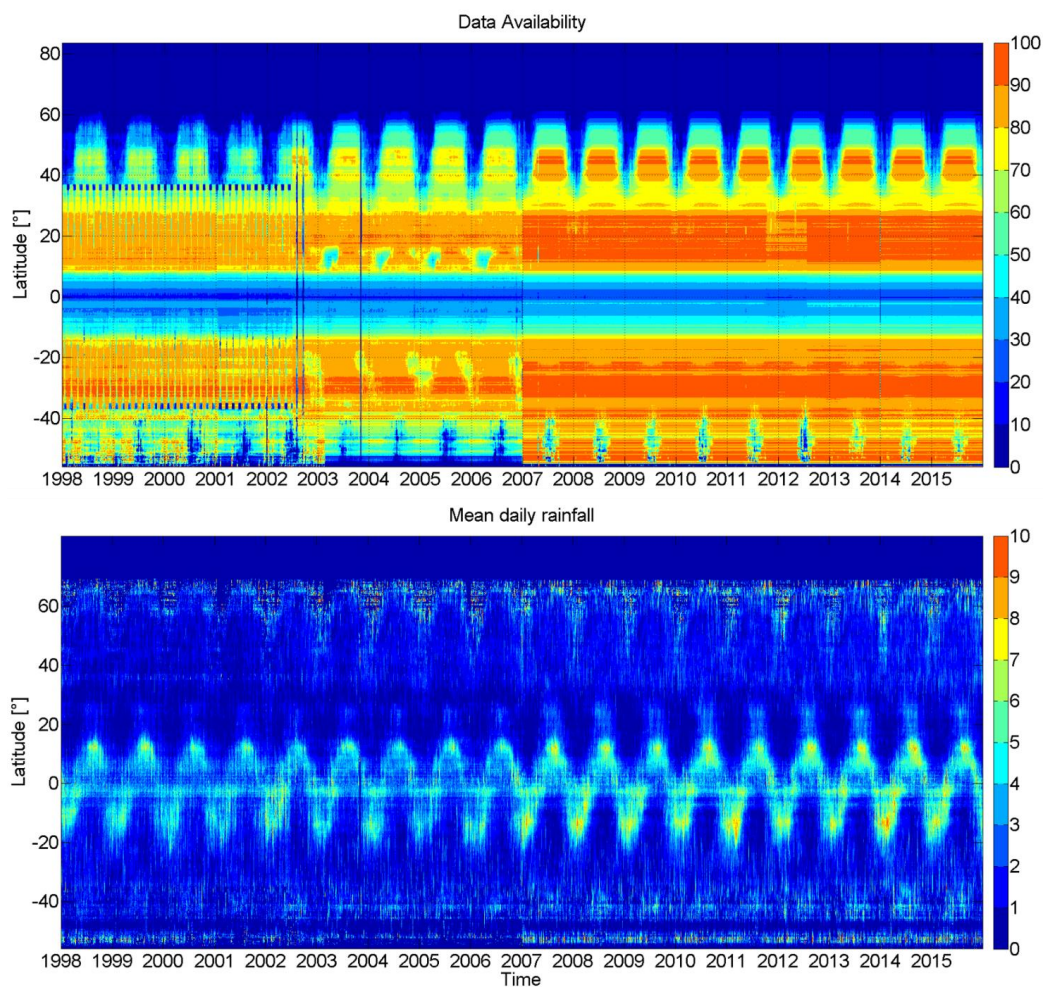
514 **Figure 1 – Data mask used for remove areas (red areas) characterized by issues in the soil moisture retrieval.**



515

516 **Figure 2 - Analysis framework.**

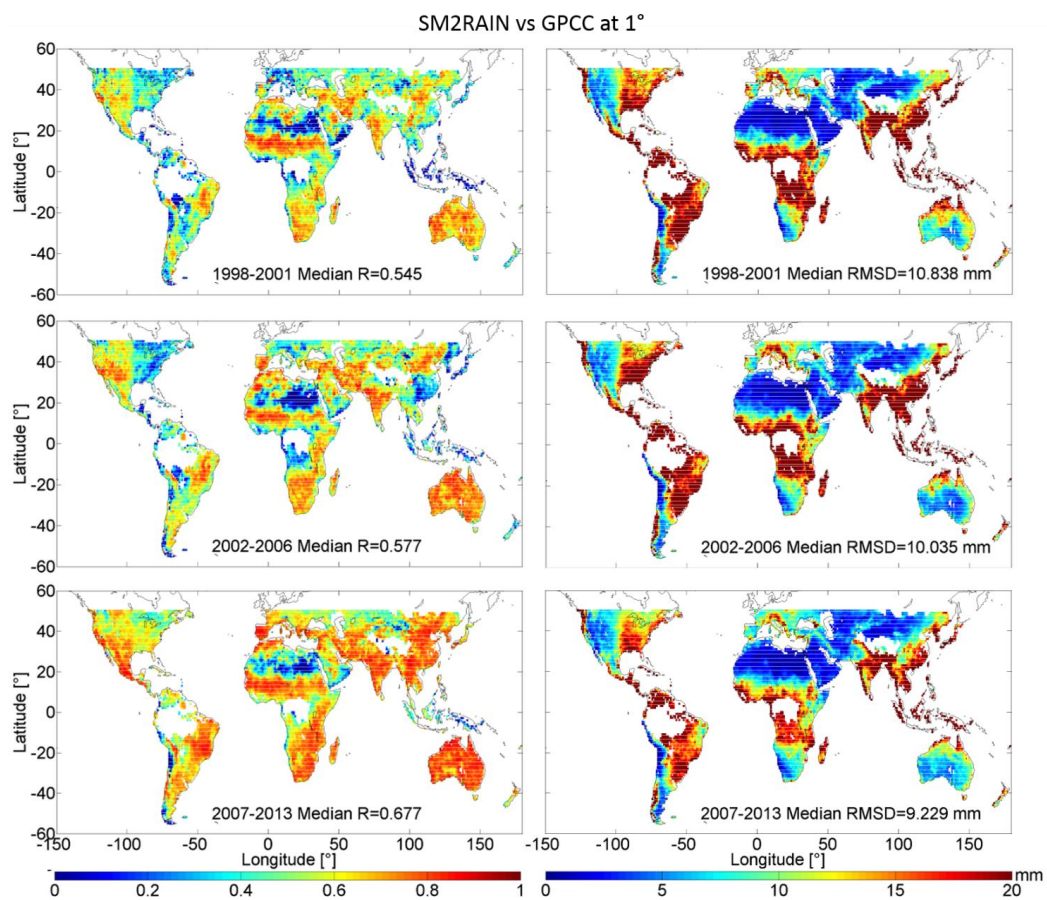
517



518

519 **Figure 3 – Hovmöller plot showing the spatial-temporal data availability, in percentage of the total annual available data**
520 **(upper panel) and the mean daily rainfall (lower panel) of the SM2RAIN-CCI rainfall data set for different latitude bands.**

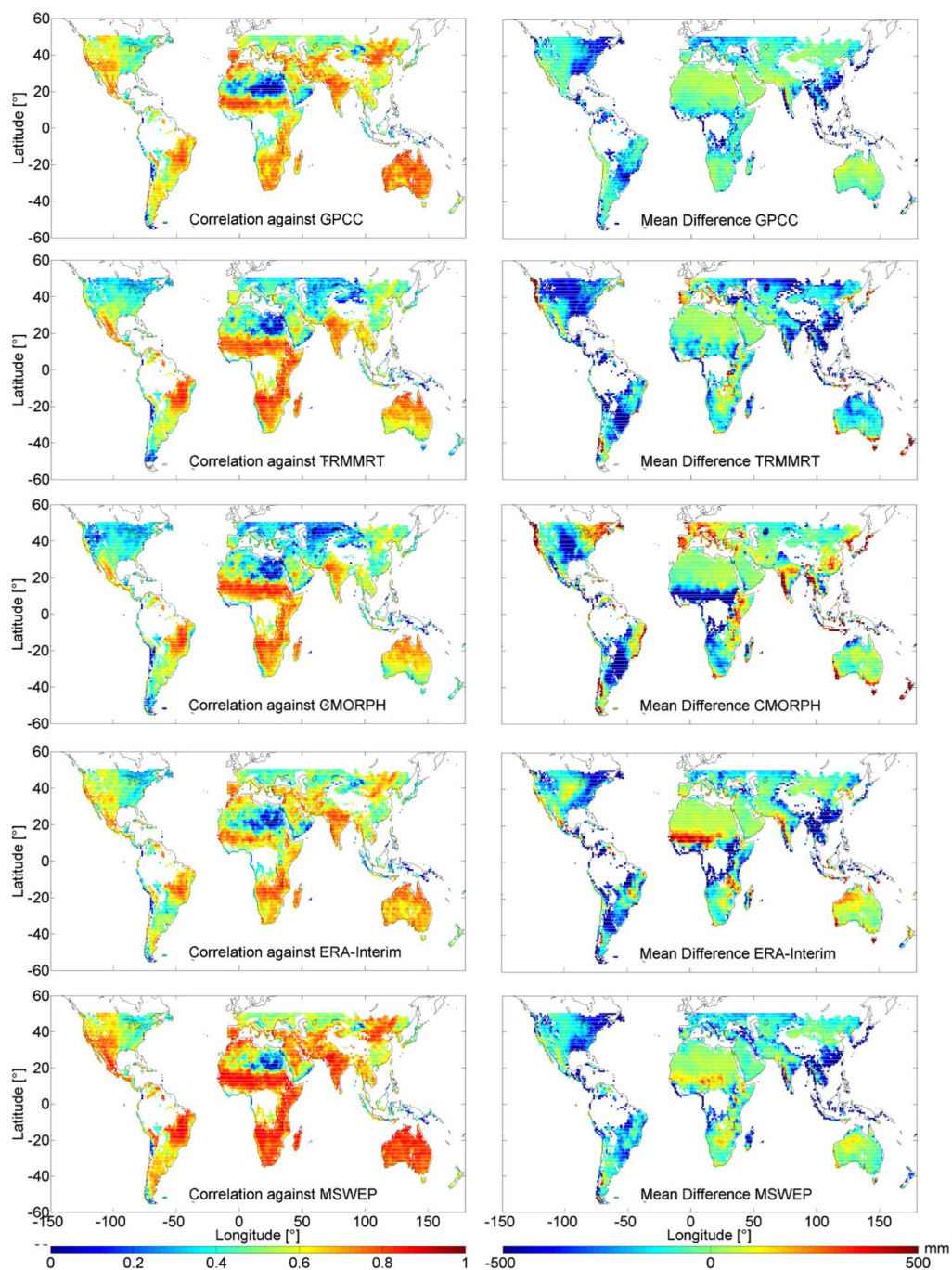
521



522

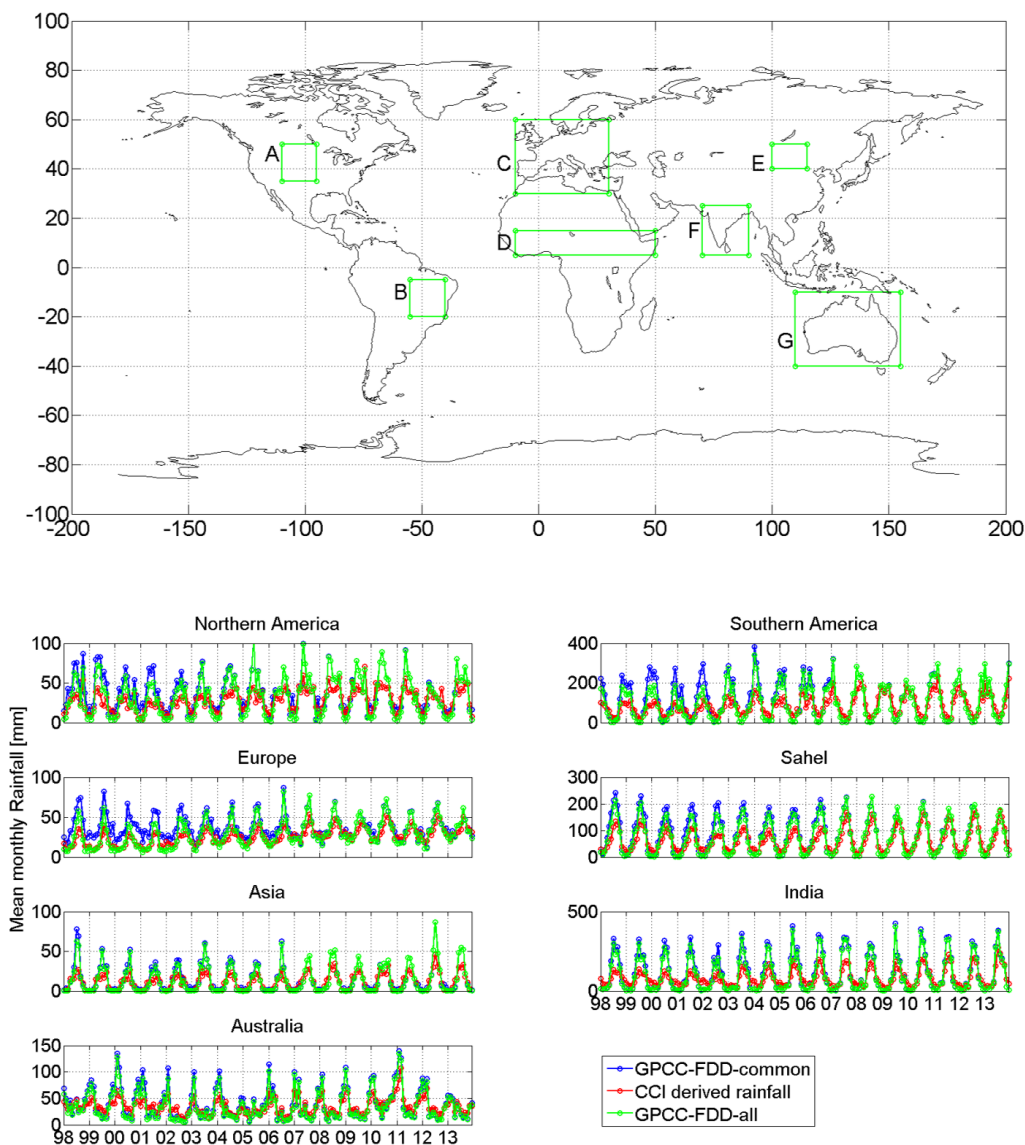
523 **Figure 4 – Global Pearson correlation (left) and Root Mean Square Difference (right) maps obtained between GPCC-FDD**
 524 **and the SM2RAIN-CCI rainfall data set for 5-day accumulated rainfall during the periods 1998-2001 (upper panel), 2002-**
 525 **2006 (middle panel) and 2007-2013 (lower panel).**

526



527

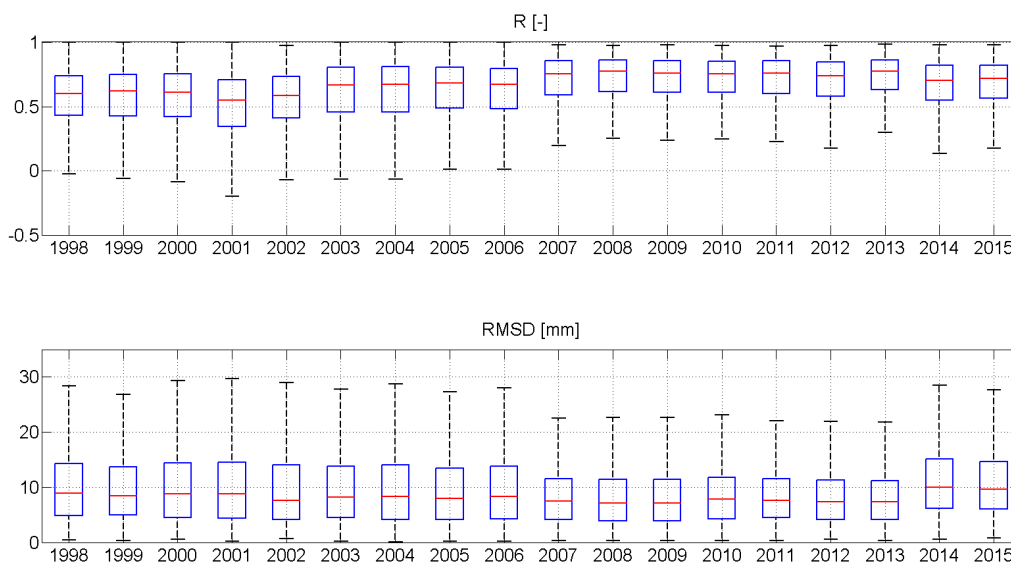
528 **Figure 5 – Correlation maps for 5 days of accumulated rainfall (left column) and differences in mean annual rainfall (right**
 529 **column) obtained by comparing (from top to bottom) SM2RAIN-CCI and GPCC (a), SM2RAIN-CCI and TRMMRT (b),**
 530 **SM2RAIN-CCI and CMORPH (c), SM2RAIN-CCI and ERA-Interim (d) and SM2RAIN-CCI and MSWEP (e) at 1° of**
 531 **spatial resolution.**



532

533 **Figure 6 – Mean Monthly Rainfall estimated by GPCC-FDD (blue line) and the new CCI-derived rainfall data set (red line)**
 534 **over the six analysis boxes throughout North America (A), South America (B), Europe (C), Sahel (D), Asia (E), India (F) and**
 535 **Australia (G) during the period 1998-2013. The blue lines draw the Mean Monthly Rainfall estimated by GPCC-FDD when**
 536 **both a ground-based and a SM-derived rainfall estimate is available.**

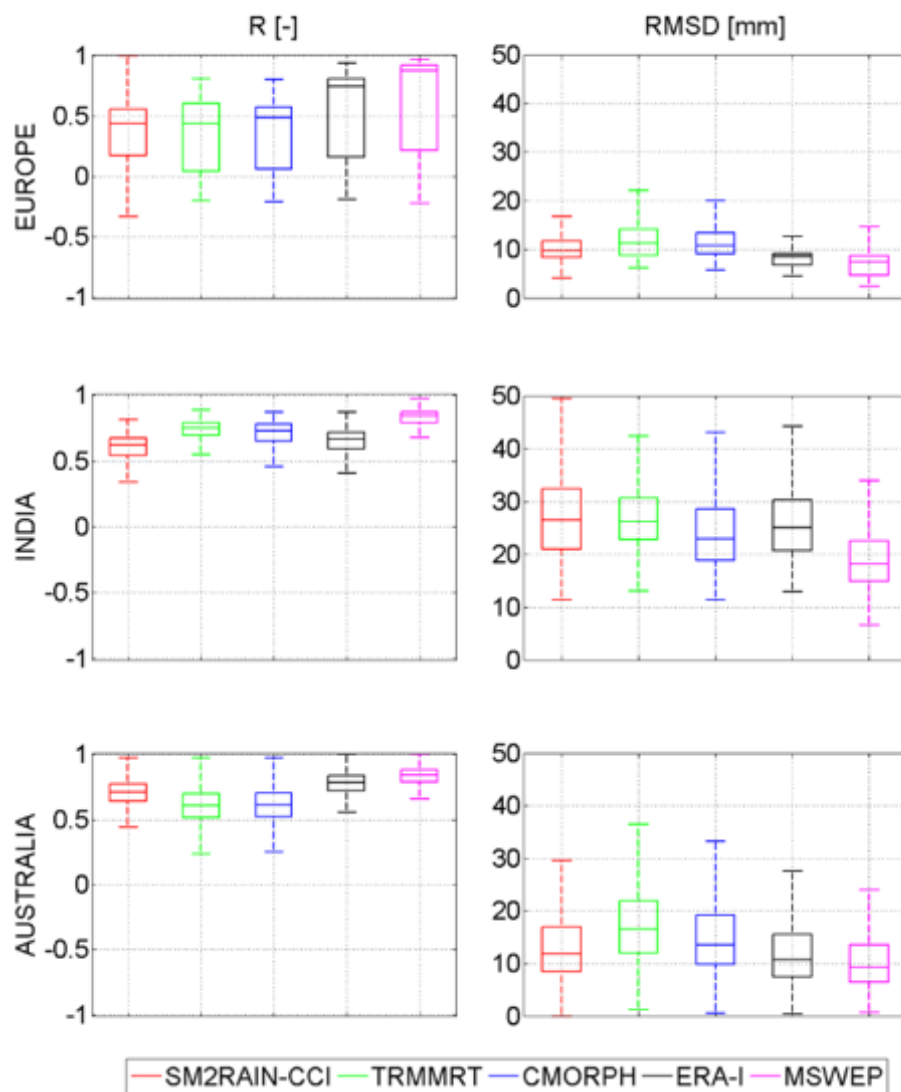
537



538

539 **Figure 7 – Yearly boxplots for the correlation coefficients (R) and Root Mean Square Differences (RMSD, in mm) between**
540 **SM2RAIN-CCI and MSWEP obtained on a global scale at 0.25° spatial resolution during the period 1998-2015. For each box,**
541 **the red line represents the median values, the blue box the 25th and 75th percentile, while the black dotted whiskers extend to**
542 **the most extreme data points.**

543



544

545 **Figure 8 – Correlation coefficient (left) and Root Mean Square Difference (RMSD, right) box plots obtained by comparing**
 546 **SM2RAIN-CCI (in red), TRMMRT (in green), CMORPH (in blue), ERA-Interim (in black) and MSWEP (in magenta) with**
 547 **gauge-based data sets over Europe (top), India (middle) and Australia (bottom).**

548